Hindawi
International Journal of Antennas and Propagation
Volume 2019, Article ID 9285476, 14 pages
https://doi.org/10.1155/2019/9285476

*Research Article*

# Design of Wideband Slot Antenna Array with Stereoscopic Differentially Fed Structures

**Guang Sun**,[1] **Ge Gao**,[1] **Tingting Liu**,[2] **Yi Liu**,[1] **and Hu Yang**[1]

[1]*College of Electronic Science and Technology, National University of Defense Technology, 410073 Changsha, China*
[2]*Science and Technology on Blind Signal Processing Laboratory, Southwest Electronics and Telecommunication Technology Research Institute, Chengdu 610041, China*

Correspondence should be addressed to Yi Liu; yi_liu@nudt.edu.cn

Received 25 March 2019; Revised 4 June 2019; Accepted 17 June 2019; Published 1 August 2019

Academic Editor: Hervé Aubert



In this paper, a wideband slot antenna element and its array with stereoscopic differentially fed structures are proposed for the radar system. Firstly, a series of slots and a stereoscopic differentially fed structure are designed for the antenna element, which makes it possess a wide bandwidth, stable radiation characteristics, and rather high gain. Moreover, the stereoscopic feeding structure can firmly support the antenna's radiation structure and reduce the influence of feeding connectors on radiating performance. Secondly, a $4 \times 4$ array is designed using the proposed antenna element. And a hierarchical feeding network is designed for the array on the basis of the stereoscopic differentially fed structure. For validation, the antenna element and $4 \times 4$ array are both fabricated and measured: (1) the measured −10 dB impedance bandwidth of the antenna element is 62% (6.8–12.9 GHz) and the gain within the entire band is 5–9.7 dBi and (2) the measured −10 dB impedance bandwidth of the array is approximately 50% (7 to 12 GHz) with its gain being 14–19.75 dBi within the entire band. Notably, measured results agree well with simulations and show great advantages over other similar antennas on bandwidth and gain.

## 1. Introduction

In recent years, radar systems have received widespread attention for their ability to detect, identify, and monitor a variety of targets. Many of their most recent advances include system miniaturization, a reduction in overall weight, and an increase in performance rate. In particular, the development of high-performance antennas with wider bandwidths, higher gain, and stable radiation patterns is promising for vital applications in radar systems. Microstrip slot antennas have been widely studied and applied to many radar systems because of many advantages like their lightweight, low profile, low cost, and ease of integration [1, 2]. However, the bandwidth of traditional microstrip slot antennas is rather narrow. Therefore, there is great interest in the design of microstrip slot antennas with high gain and wide bandwidth for the side-fire antenna array that are optimized for radar systems [3–5]. Apart from traditional microstrip slot antennas, tapered slot antennas [6, 7] have a wide operating bandwidth, but they are end-fire antennas and have a large longitudinal dimension. Therefore, it is difficult to be used for side-fire antenna arrays.

To expand the bandwidth of slot antennas, various techniques have been employed. A direct method is using multiple narrow slots with different lengths [8]. The radiating slots are designed with three unequal arms in length fed by coplanar waveguides, as in [8], to produce three distinct resonances. And a wide impedance bandwidth can be realized by combining different resonance sources. Modifying the form or structure of the radiating slot is another way to expand the bandwidth. This process mainly includes adding shorting vias, loading parasitic patches, or increasing coupling slots [9–13]. In [9], with the shorting vias loading, the lowest mode in the substrate integrated waveguide (SIW) cavity is shifted upward and coupled with two higher order modes. Therefore, a wide bandwidth that includes three resonances is realized. Another similar wideband stacked patch antenna is designed in [14], and the

antenna enhances the coupling between an excited dipole and an unexcited dipole by introducing four fan-shaped parasitic patches. By changing the antenna's resonant mode, this method can extend the bandwidth to 51%. However, the configurations of these antennas mentioned above are intricate, which increases the difficulty of designing feeding structures to achieve good impedance matching. Acting as a simple radiation structure, wide slots are widely used to design wideband antennas. Cavity-backed slot antennas (CBSAs) have the advantages of large bandwidth and high gain. In [15], a rectangular wide slot is applied, along with a metal cavity, to design a CBSA, which achieves a wide impedance bandwidth of 40% and high gain of 8 dBi. However, its array has only the impedance bandwidth of 30%. Similar work can also be found in papers [16–18]. But it should be noted that the reported CBSAs do not exceed a 40% impedance bandwidth. In addition, these antenna structures are costly and have a complicated fabrication process. To extend the antenna's bandwidth, increasing the width of the slots is a good way. However, on the contrary, wider bandwidth may cause schismatic or asymmetric radiation patterns [19].

The differentially fed structures can excite the antenna through differential signals with equal amplitude and opposite phase. Therefore, this method of applying differential signals to excite antennas is an effective way to stabilize antenna patterns by suppressing cross-polarization levels while maintaining the broadband characteristic of the antenna. Moreover, the feeding structure can be directly connected to the differential circuits without an additional balun and is easy to realize full integration. By adopting differential feeding, via two coplanar ports, a wideband ring slot antenna is designed in [20], which achieves a 51% bandwidth with a stable radiation pattern within the operational bandwidth. However, the coplanar differentially fed structure increases the size of the antenna and cannot be used to integrate a differentially fed antenna array. In [21], the coupled dipole array with wideband differential feeding has a wide operating bandwidth. But its differential feeding structure is complex, and a feeding network cannot be designed for antenna array integration.

To satisfy the high-gain requirements of radar systems, a $4 \times 4$ planar array needs to be further investigated in this paper. However, the $4 \times 4$ differentially fed arrays are rarely proposed because of the difficulty of designing differential feeding networks. Therefore, it is a key challenge to design an appropriate feeding network for the differentially fed array.

In this paper, a wideband differentially fed planar circular slot antenna element and a $4 \times 4$ antenna array are designed based on the stereoscopic feeding structures. The proposed antenna has triple resonance in its operation bands. The triple-resonance antenna is analyzed with its field distributions and surface current distribution. With two rectangular slots loading, a lowest mode is created and coupled with two higher order modes. Therefore, a wide bandwidth with triple resonance is realized. To achieve a stable wideband radiation pattern, a stereoscopic differentially fed structure is introduced, and it can also avoid the influence of the joint and exciting components on the antenna's performance and plays an important role in supporting the antenna structure. And based on the stereoscopic feeding structures, a hierarchical feeding network is designed to solve the problem of designing wideband differentially fed antenna arrays. Finally, to further validate the capability of the proposed antenna, an antenna element and a $4 \times 4$ antenna array are designed, fabricated, and tested.

## 2. Antenna Configuration

Figure 1 shows the configuration of the proposed wideband differentially fed slot antenna. The proposed antenna consists of three components: the radiating part, the feeding part, and the ground plane. An exploded view of the proposed circular slot antenna is illustrated in Figure 2. The radiating part consists of a two-layer F4BM substrate with a relative permittivity $\varepsilon_r$ of 2.2 and a loss tangent of 0.0007. The thickness of the single-layer F4BM substrate is 1 mm. Multiple radiating slots are etched on the top and bottom layers of the double substrate. The circular slot is the main radiating structure, and two rectangular slots printed on the bottom layer of the substrate are used to expand antenna bandwidth and connect the feeding structures. The two-layer grounded substrate with a central conductor strip forms a strip line, which is used to feed the radiating slots. The feeding part consists of a pair of stereoscopic feeding structures formed by strip lines. To realize the differential feeding, two differential ports (designated as port 1(+) and port 2(−)) shown in Figure 1(b) are connected with the differential circuit via two 50 Ω SMA connectors, which use two equal-amplitude and reverse-phase signals to excite the antenna. The vertical strip lines and the horizontal strip lines are connected by using two rectangular holes dug in the lower substrate of the radiating part and two bumps added on the outer substrates of the feeding part, as shown by the dotted line in Figure 2. The thickness of the coating metal is 0.035 mm. The metal vias with a diameter $d_v$ of 0.25 mm and a pitch $d_f$ of 0.45 mm are arranged in rows at the end of the feeding lines, which serve as an extension of the metal ground to ameliorate the grounding discontinuity, which improves the impedance characteristics. To obtain a unidirectional radiation pattern, the proposed antenna is fixed above a square-shaped reflecting plane. Both the feeding network and the antenna part are designed with strip line components to reduce the transmission loss and mutual coupling between the complex feeding networks. Finally, two differential ports are adopted to excite the slots through the stereoscopic feeding structures. The dimensions of the proposed antenna are optimized with CST Microwave Studio 2018.

## 3. Antenna Design and Analysis

*3.1. Design Process.* The evolution of the proposed antenna is shown in Figure 3, and the corresponding reflection coefficients, gains, and radiation patterns are displayed in Figures 4 and 5. In general, the impedance bandwidth of these conventional slot antennas is very narrow because of the limitations of the structure. However, former research demonstrates that the adoption of wide slots in antenna

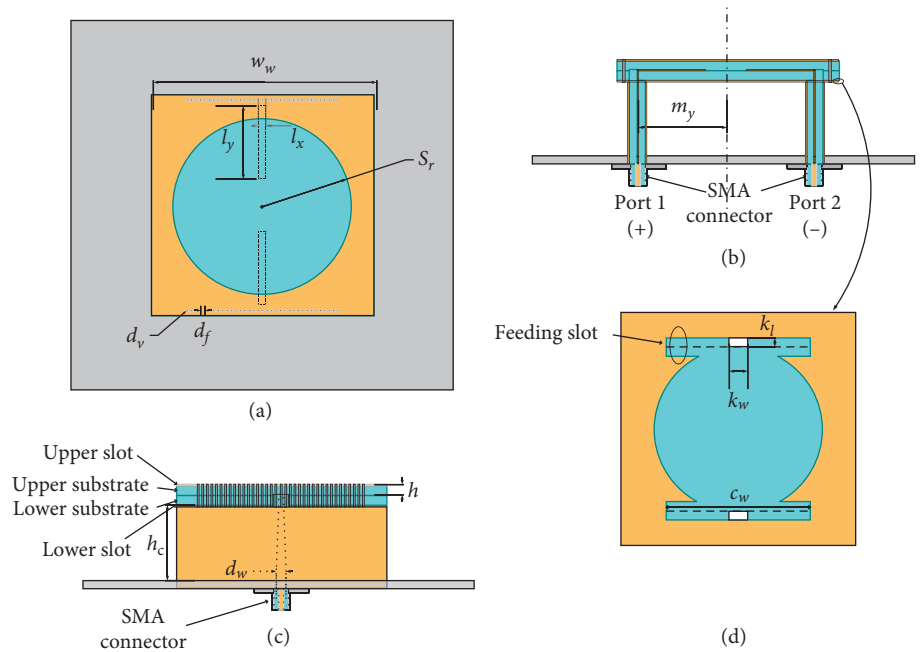


FIGURE 1: Configuration of the proposed circular slot antenna (unit: mm; $w_w = 25$, $m_y = 21$, $s_r = 10.2$, $l_x = 0.4$, $d_w = 1.3$, $l_y = 8$, $h_c = 8$, $c_w = 16$, $h = 1$, $d_v = 0.25$, $d_f = 0.45$, $k_w = 1$, $k_l = 1$). (a) Top view. (b) Front view. (c) Left view. (d) Lower-layer slot and feed slot.

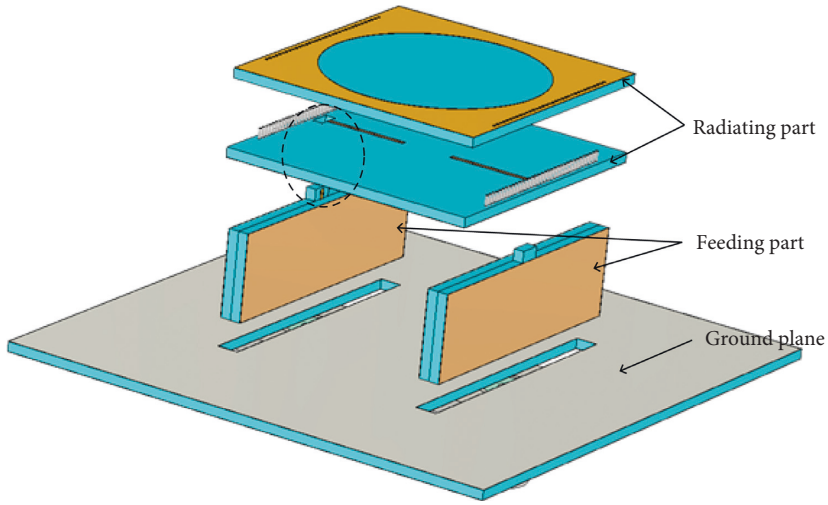


FIGURE 2: Exploded view of the proposed circular slot antenna.

design is a simple and effective approach to achieve wide bandwidth. Thus, to achieve a wide impedance bandwidth, a circular slot is introduced. First, we design the antenna, which is marked as Ant. 1 and shown in Figure 3(a). Ant. 1 can develop two resonant frequencies which are marked as $f_1$ and $f_2$, but the impedance bandwidth is limited. In addition, an obvious beam deflection in the E-plane and beam splitting in the H-plane occur at the higher frequency band because of the asymmetry of the feeding structure, as shown in Figure 5. To obtain a stable wideband radiation pattern, another feedline is introduced in Ant. 2. The differential feeding is achieved with two feedlines. The benefit can also be seen in Figure 4(a) after differential feeding is introduced. Therefore, both the resonant frequencies $f_1$ and $f_2$ move towards lower frequencies because of the influence of the feeding phase between the two differential feedlines. Meanwhile, two resonance points move closer to each other, and the impedance matching is improved. From Figure 5, it also can be found that the radiation patterns in Ant. 2 have been greatly improved and significant beam deflection and splitting disappeared. But there is still a slight deflection in the E-plane. To expand the bandwidth of the proposed antenna and further stabilize the antenna's patterns, a stereoscopic feeding structure and two rectangle slots are introduced in Ant. 3. Two rectangle slots are etched onto the bottom of the double substrate to expand the bandwidth of Ant. 3, which excites an additional resonant mode at lower frequencies. By combining multiple resonant modes, a wide impedance bandwidth is obtained. Furthermore,

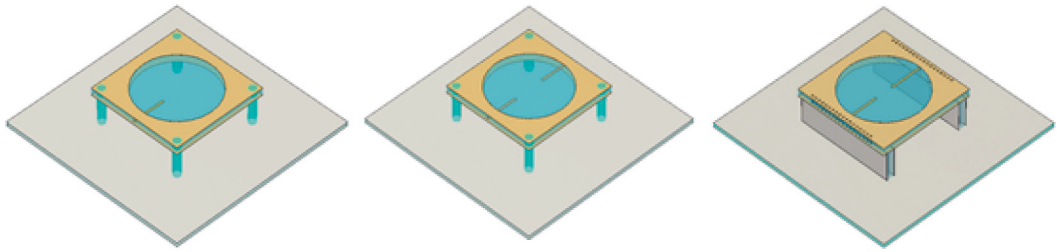


Figure 3: Evolution of the proposed antenna (Ant. 1: single feeding antenna; Ant. 2: differentially fed antenna; Ant. 3: stereoscopic differentially fed antenna).

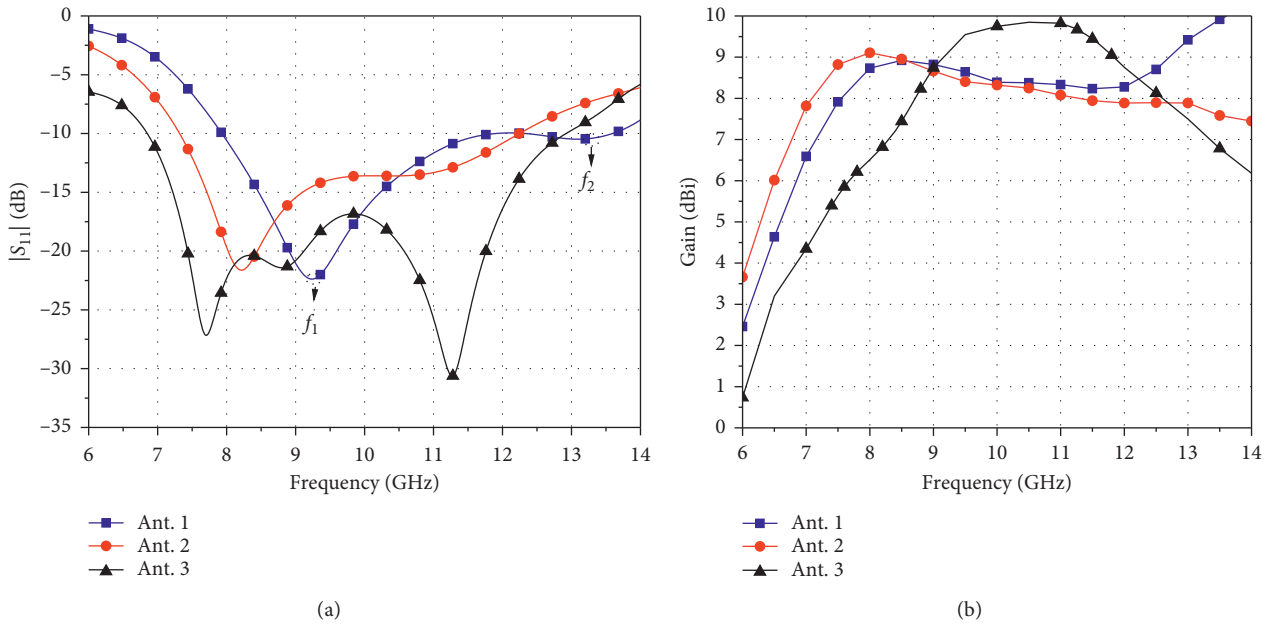


Figure 4: Simulated active reflection coefficients $|S_{11}|$ (a) and gains (b) in the evolution of the antennas.

as shown in Figure 4(b), the gain of the proposed antenna with a stereoscopic feeding structure is significantly improved within the bandwidth of 9–12 GHz. The electrical field distribution, between the radiation slot and metal reflective surface, is more concentrated because of the stereoscopic feeding structure.

*3.2. Character Analysis of the Proposed Antenna.* To better understand the working mechanism of differential feeding of Ant. 3, the E-field distribution of a circular slot aperture with single feeding and differential feeding is shown in Figures 6(a) and 6(b), respectively. As shown in Figure 6(a), the cross-polarized components in the H-plane are generated because of the asymmetrical structure of the single-fed slot antenna. When another feedline is added, the antenna is excited by differential signals, and the E-field distributions in the circular slot become symmetric, as shown in Figure 6(b); this leads to two equal-amplitude and reverse-phase cross-polarized components in the H-plane. The cross-polarized radiations can be effectively cancelled out. Thus, the radiation patterns are improved. In conclusion, the differential feeding reduces the cross-polarization. And simultaneously, stable radiation patterns and high gain are obtained in the main radiation direction.

To better explain the wideband working mechanism and radiation characteristics of the proposed Ant. 3, the current and E-field distributions of the proposed antenna at three different resonant points (7.68 GHz, 8.86 GHz, and 11.26 GHz) are shown in Figures 7(a)–7(f). The resonant frequency is mainly determined by the electrical length of the slots. As shown in Figure 7(a), the current distribution of the first mode (at 7.68 GHz) mainly concentrates on the edges of two rectangular slots and circular slot etched on the bottom of the substrate. The introduction of the two rectangular slots increases the length of the current path and causes the proposed antenna to generate a new resonant mode at 7.68 GHz. Figures 7(b) and 7(e) depict the current and E-field distributions of the second resonant mode at 8.86 GHz. The current distribution is mainly concentrated on the edges of the circular slot. We can observe that the circular slots are excited with the differential signal with the same amplitude and opposite phase, which produces the TE11 mode at the circular aperture. Figures 7(c) and 7(f) represent the current

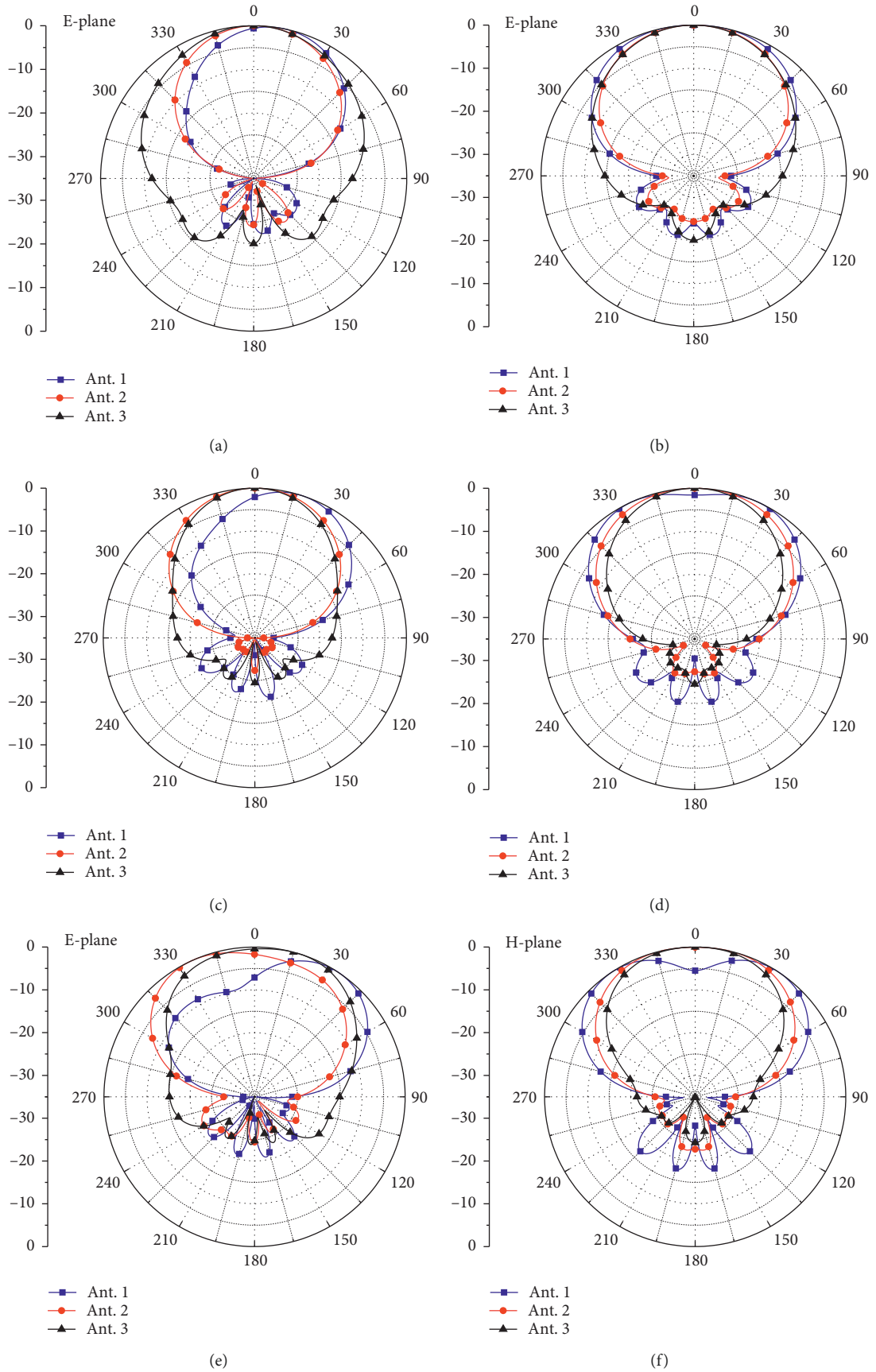


Figure 5: Simulated radiation patterns in the evolution of the antennas at different frequencies. (a) E-plane at 8 GHz. (b) H-plane at 8 GHz. (c) E-plane at 10 GHz. (d) H-plane at 10 GHz. (e) E-plane at 12 GHz. (f) H-plane at 12 GHz.

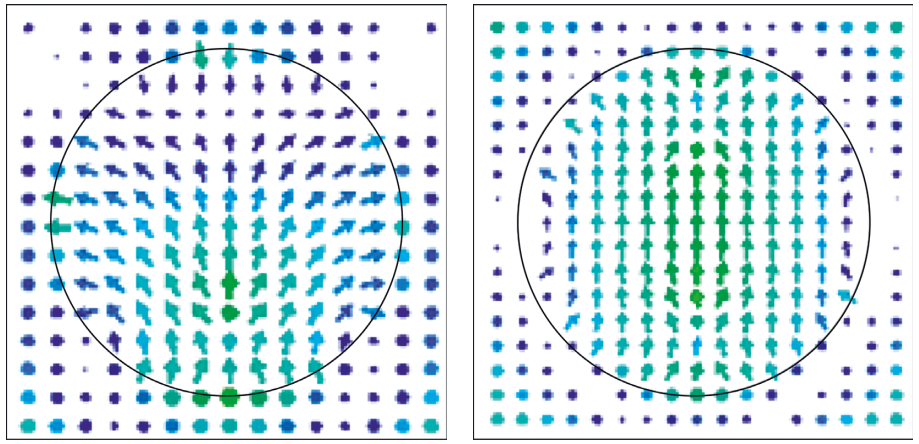

(a) (b)

Figure 6: E-field distribution at 10 GHz of (a) a single-fed antenna and (b) a differentially fed antenna.

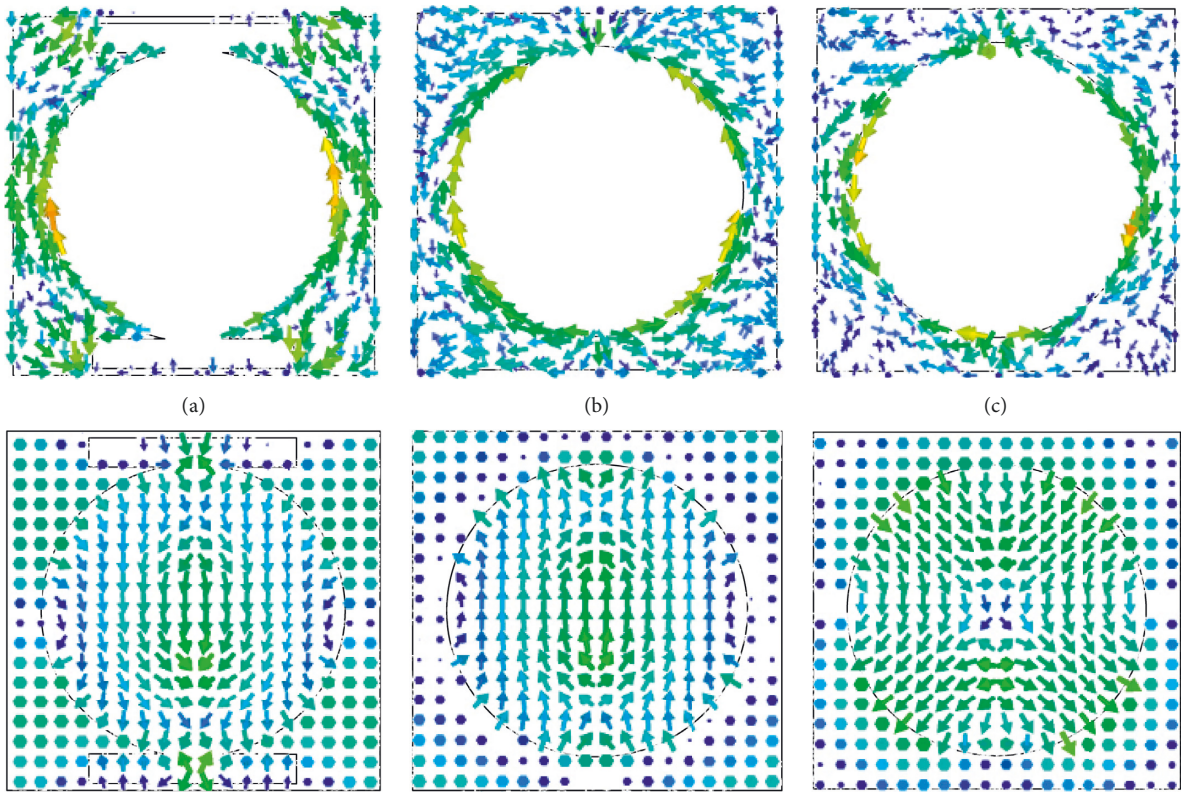

(a) (b) (c)

(d) (e) (f)

Figure 7: E-field distribution and surface current distribution of the proposed antenna at (a, d) 7.68 GHz, (b, e) 8.86 GHz, and (c, f) 11.26 GHz.

and the E-field distributions of the third resonant mode at 11.26 GHz. This shows that the resonant mode is also produced by the circular slot. When the circular slot is excited with differential signals, the high-order resonant mode of TE21 is generated at 11.26 GHz. Thus, the impedance bandwidth is broadened by combining the three modes of the proposed antenna.

To better explain the gain variation of the Ant. 3, the near E-field distribution of the antenna without stereoscopic feeding structures (Ant. 2) and with stereoscopic feeding structures (Ant. 3) is shown in Figure 8. The antenna without stereoscopic feeding structures could support the entire electric field distribution on the top of the reflective plane, as shown in Figure 8(a). When the stereoscopic feeding structure

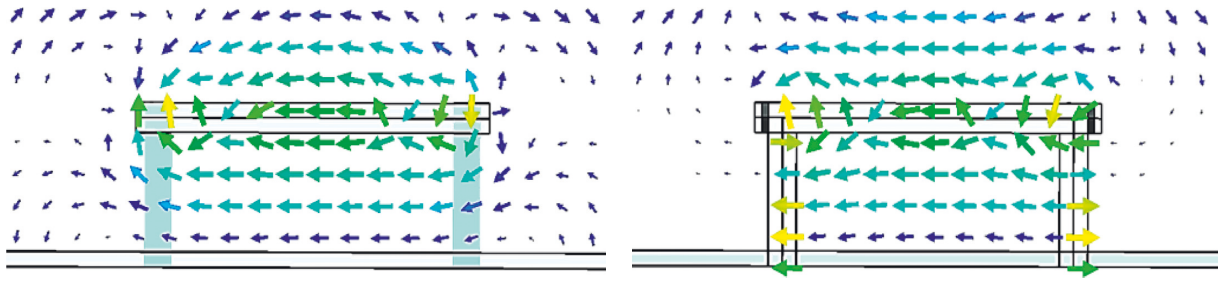


Figure 8: Near E-field distribution of the antenna in the E-plane at 10 GHz (a) without stereoscopic feeding structures and (b) with stereoscopic feeding structures.

is adopted, an equivalent semiclosed cavity is formed together with the metal reflective plane. The stereoscopic feeding structures limit the electrical field into the semiclosed cavity, and the near E-field distribution on the top of the reflective plane is enhanced, as shown in Figure 8(b). The enhanced electric field distribution significantly enhances the aperture efficiency of the proposed antenna. Therefore, the beamwidth of the antenna becomes narrow and the gain is increased within the bandwidth of 9–12 GHz. However, the stereoscopic feeding structures can only work within a narrow bandwidth. On the radiation aperture surface, a part of the electric field reflected from stereoscopic feeding structures is offset at 8 GHz because of the opposite direction of the electric field. Therefore, the radiation efficiency of the proposed antenna is reduced, and the gain is decreased. Simultaneously, the introduction of the stereoscopic feeding structure reduces the equivalent radiation aperture of the antenna at lower frequencies in the E-plane, which increases the beamwidth of the patterns and decreases the gain of the proposed antenna. Despite this, the gain of the proposed antenna is high at the X-band, and the 3 dB gain bandwidth of the proposed antenna is 52%. More importantly, the stereoscopic feeding structures can improve the antenna bandwidth and are beneficial to the design of the antenna array.

*3.3. Parametric Study of Antenna Elements.* In order to investigate the effects of the design parameters on the impedance bandwidth of Ant. 3, some key parameters are evaluated, as shown in Figures 9–12. Only one parameter is studied at a time, while the other parameters are fixed.

Figure 9 shows the frequency behavior of $|S_{11}|$ of the proposed antenna for different values of parameter $S_r$. According to Figure 9, when $S_r$ increases from 9.7 to 11.2 mm, the resonant frequency of the second and third resonance points moves to lower frequencies and impedance matching is improved, but the impedance bandwidth decreases at higher frequencies. This means that the parameter $S_r$ plays an important role in controlling the second and third resonant frequency points, the impedance matching, and the bandwidth of the proposed antenna. To obtain a wide impedance bandwidth and good impedance matching, the value of the parameter $S_r$ is chosen to be 10.2 mm.

To observe the effect of two extra parasitic slots on the antenna impedance bandwidth of Ant. 3, the length $c_w$ is

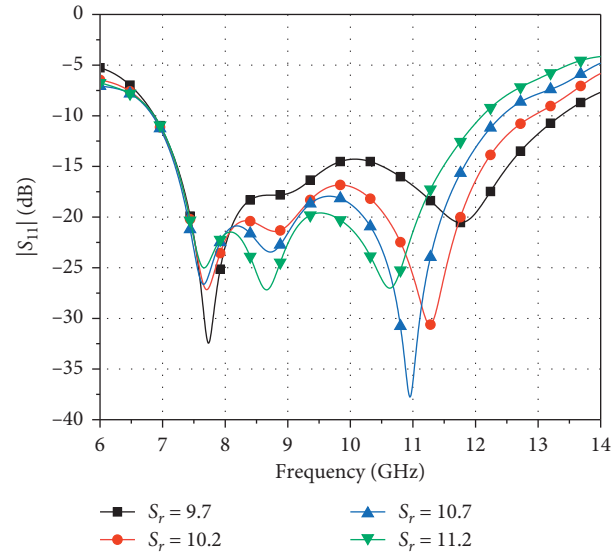


Figure 9: Simulated differential reflection coefficient versus parameter $S_r$ ($S_r$ = 9.7 mm, $S_r$ = 10.2 mm, $S_r$ = 10.7 mm, $S_r$ = 11.2 mm).

evaluated. As shown in Figure 10, the lower resonant frequency moves toward the higher frequency as the length $c_w$ of the rectangular slots decreases. When the length $c_w$ is reduced to 10 mm, the first resonant point disappears, whereas the second resonant frequency changes slightly and the third resonant point remains unchanged, as is shown in Figure 8. Therefore, this means that $c_w$ plays a crucial role in controlling the first resonant frequency. It can be explained that the introduction of two extra parasitic slots increases the current path length of the radiation aperture and causes the proposed antenna to generate a new resonant mode at lower frequencies. To obtain a wide operating bandwidth, $c_w$ = 16 is selected.

The dimension of the feedline is studied in Ant. 3, as shown in Figure 11. It is observed that when the feedline length $l_y$ increases, the curve of $|S_{11}|$ goes up in the lower frequency bands and goes down in the higher frequency bands; this suggests that the feedline length $l_y$ has a great effect on impedance matching. To obtain a good impedance match, the optimal feedline length $l_y$ is set to 8 mm.

In the process of designing an antenna element with a metal reflector, the dimension of the metal reflecting surface

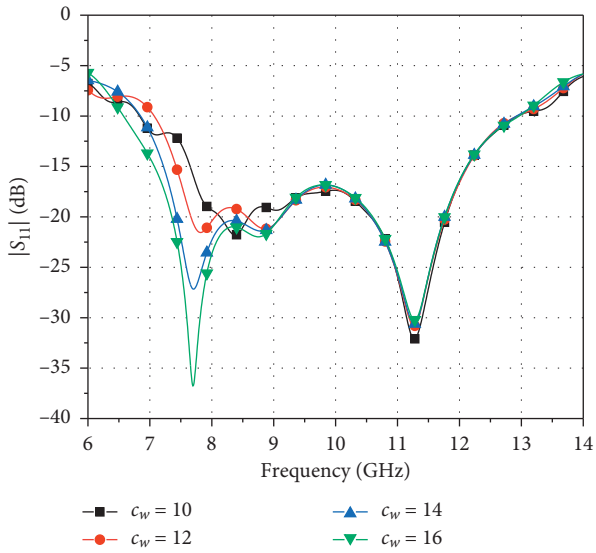


Figure 10: Simulated differential reflection coefficient versus parameter $c_w$ ($c_w$ = 10 mm, $c_w$ = 12 mm, $c_w$ = 14 mm, $c_w$ = 16 mm).

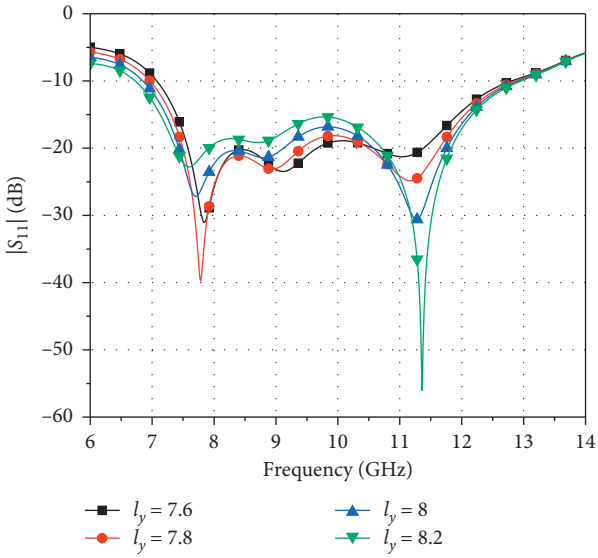


Figure 11: Simulated differential reflection coefficient versus parameter $l_y$ ($l_y$ = 7.6 mm, $l_y$ = 7.8 mm, $l_y$ = 8 mm, $l_y$ = 8.2 mm).

has less influence on the performance of the antenna array, so it is not optimized. But the distance $h_c$ between the slot antenna and the reflector has to be studied in Ant. 3. The frequency behavior of $|S_{11}|$ of the proposed antenna for different values of the distance $h_c$ is shown in Figure 12. We can observe that when the distance $h_c$ increases, both the lower and higher resonant frequencies shift to the lower frequency bands. This means that distance $h_c$ has a great impact on the antenna's operating frequencies. Therefore, to obtain an appropriate operating bandwidth, the distance $h_c$ is chosen to be 8 mm.

*3.4. Simulated and Measured Results of Antenna Elements.* The fabricated prototype of the proposed antenna element is shown in Figure 13. The full-wave simulated and

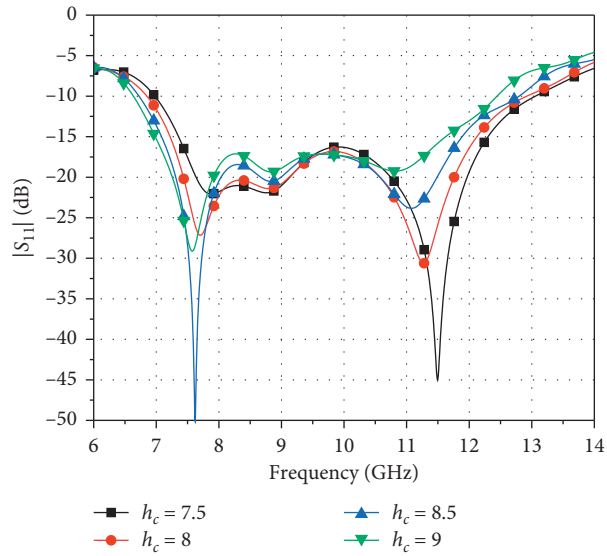


Figure 12: Simulated differential reflection coefficient versus parameter $h_c$ ($h_c$ = 7.5 mm, $h_c$ = 8 mm, $h_c$ = 8.5 mm, $h_c$ = 9 mm).

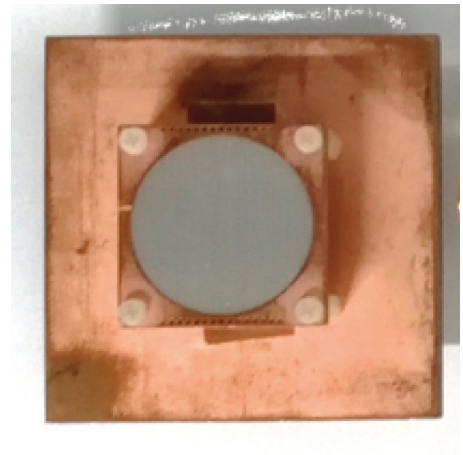

Figure 13: Photograph of the fabricated antenna element.

measured results of return loss and gains of the antenna element are shown in Figures 14(a) and 14(b), which reveals that the measured impedance bandwidth reaches 62% (6.8–12.9 GHz) for $S_{11} < -10$ dB and the simulated maximum gain is 9.7 dBi at 11 GHz. The measured results are consistent with the simulated results. But because of the fabrication accuracy and test errors, the measured resonance frequencies were slightly changed. The measured gain is about 0.5 dB lower than the simulated results at 10 GHz. The main reason for this difference is mostly due to a combination of fabrication accuracy and material loss. The impedance matching deteriorates at 10 GHz, which results in a decline in antenna radiation efficiency. Therefore, the antenna gain attenuates at 10 GHz. The radiation patterns in both the E-plane and H-plane at 7.5 GHz, 10 GHz, and 12.5 GHz are shown in Figures 15(a) and 15(b). Good unidirectional radiation characteristics and a stable radiation pattern are obtained within the entire band. Above all, in comparison with the similar previously

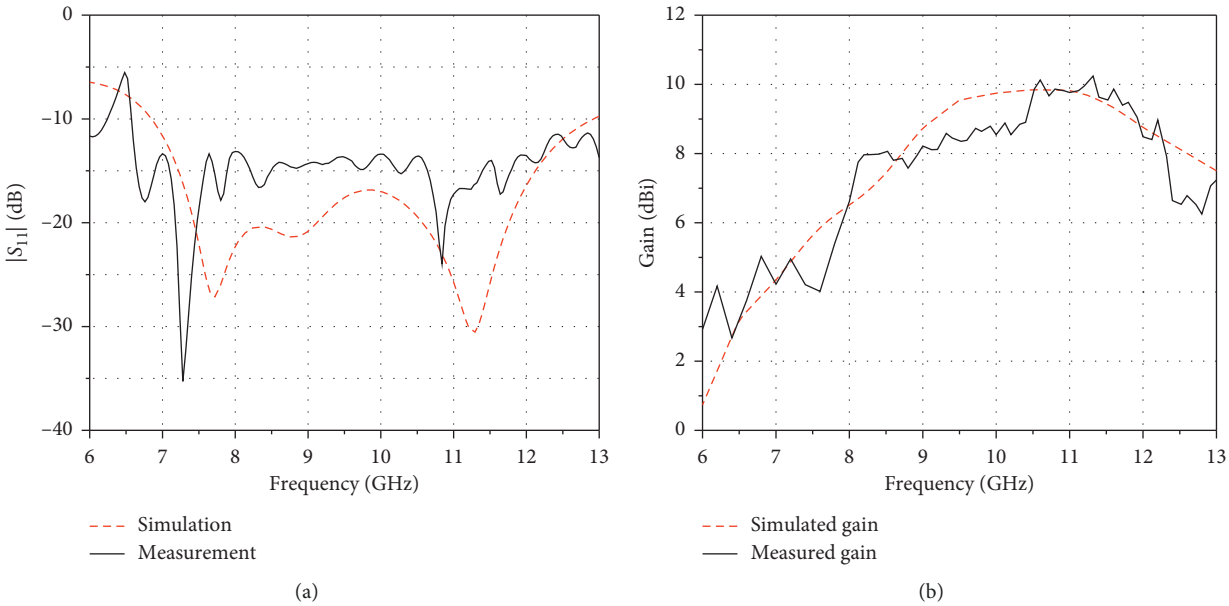


Figure 14: Simulated and measured $|S_{11}|$ (a) and gains (b) of the antenna element.

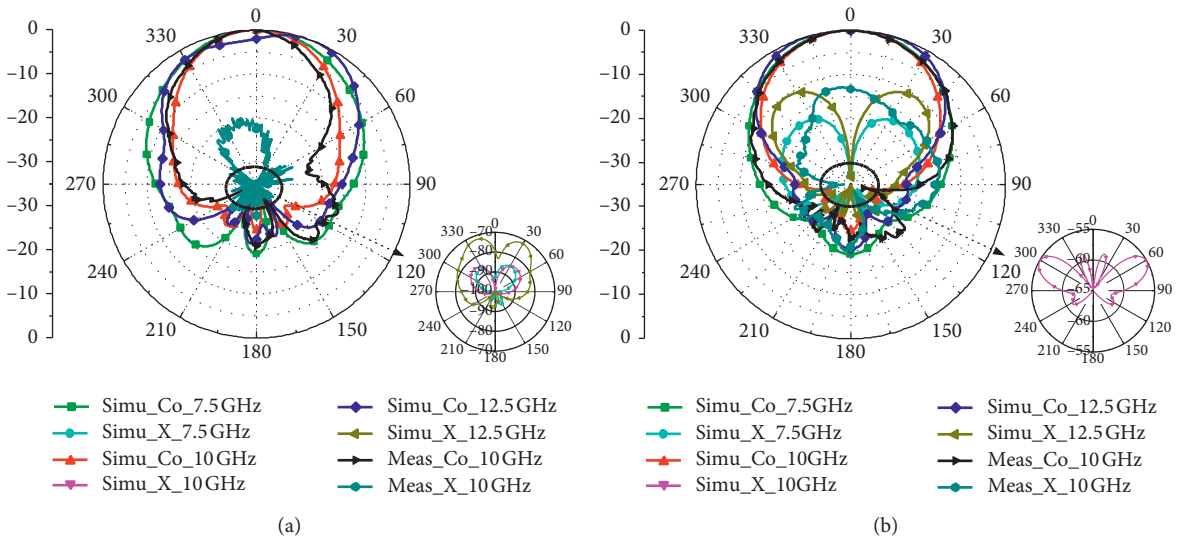


Figure 15: Simulated and measured co- and cross-polarization radiation patterns of the proposed antenna element at 7.5 GHz, 10 GHz, and 12.5 GHz. (a) E-plane. (b) H-plane.

proposed antennas [10–20], the impedance bandwidth is visibly wider.

## 4. Differentially Fed Antenna Array Design

To satisfy the requirements of high gain in radar systems, it is an effective way to design an antenna array. However, the feeding network using the traditional planar microstrip feedline layout is not satisfied for designing a $4 \times 4$ differentially fed antenna array. Therefore, to obtain a compact wideband slot antenna array for radar systems, a hierarchical feeding network based on the stereoscopic feeding structure is proposed. To obtain a higher gain and reduce the mutual coupling between antenna elements, elements are arrayed with a constant spacing of 23 mm in both $x$- and $y$-directions.

Figure 16 shows the configuration of the proposed wideband differentially fed slot antenna array. Figures 16(a) and 16(b) show the top view and front view of the antenna array, respectively. The metal vias are arranged in rows between the radiation elements that are used to reduce the mutual coupling and improve the impedance bandwidth of the antenna array. The feeding network of the proposed antenna array is shown in Figures 16(c) and 16(d), and it consists of two parts: a 1-to-4 stereoscopic feeding power divider and a 1-to-4 planar feeding power divider. The feeding network designed by using strip lines is printed on the F4BM substrate with a relative permittivity $\varepsilon_r$ of 2.2 and a

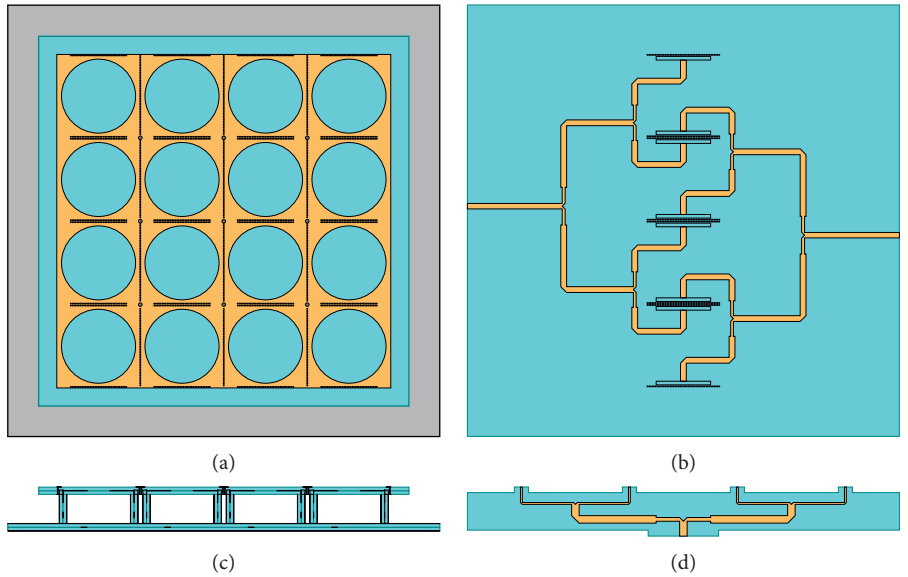


Figure 16: Configuration of the proposed antenna array. (a) Top view. (b) Front view. (c) Planar feeding power divider. (d) Stereoscopic feeding power divider.

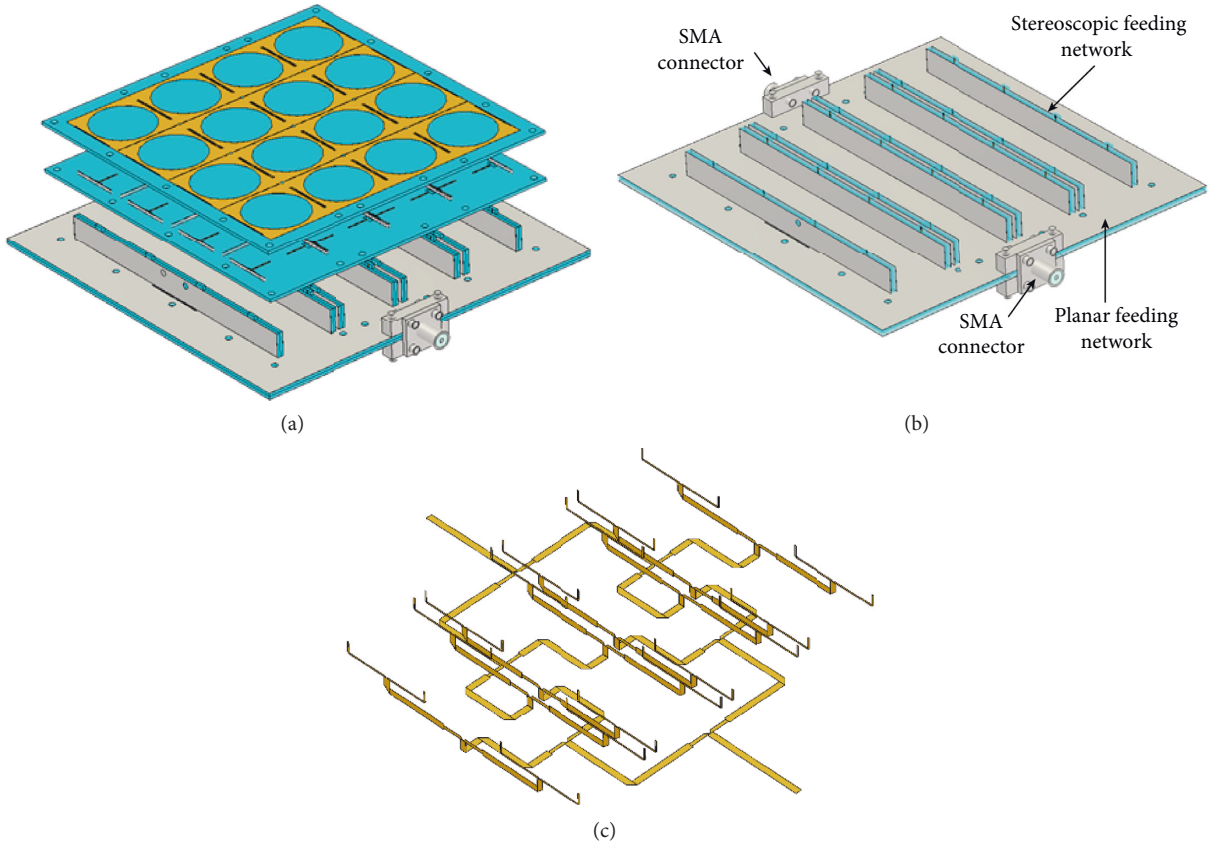


Figure 17: (a) Exploded view of the proposed antenna array. (b) Hierarchical feeding configuration of the proposed antenna array. (c) Hierarchical feeding network of the proposed antenna array.

thickness $h$ of 1 mm. The metal vias at the end of the feedline are used to ameliorate the ground discontinuity. In order to observe the array structure more clearly, an exploded view of the proposed antenna array is illustrated in Figure 17(a).

The evolution steps of the $4 \times 4$ antenna array can be divided into three steps: First, a $1 \times 4$ element line array is designed with the proposed antenna element, and the 1-to-4 power divider is designed in the two stereoscopic feeding

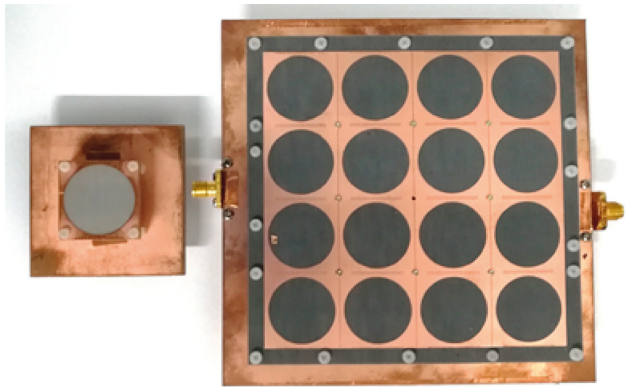

Figure 18: Photograph of the fabricated antenna element and antenna array.

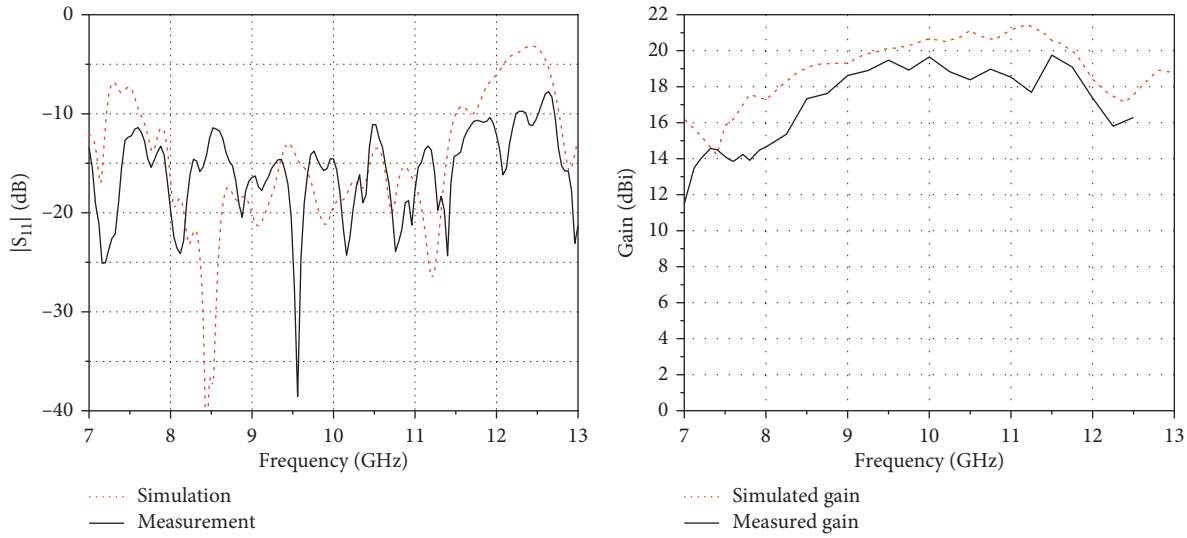


Figure 19: Simulated and measured $|S_{11}|$ (a) and boresight gains (b) of the antenna array.

structures. Then, the proposed $1 \times 4$ antenna element subarray is expanded to a $4 \times 4$ antenna array. Two planar power dividers are printed in the ground reflective plane to excite four differential ports with differential signals, respectively. Finally, the stereoscopic feeding network and the planar feeding network are integrated. To make it easier to understand the feeding structure of the $4 \times 4$ array, the hierarchical feeding configuration and the hierarchical feeding network of the proposed antenna array are shown in Figures 17(b) and 17(c). The optimal impedance match is achieved by optimizing the dimensions and structure of the proposed array.

## 5. Experimental Results

To further validate the capability of the design, a prototype of the proposed $4 \times 4$ wideband slot antenna array was fabricated and tested, as shown in Figure 18. The simulated and measured reflection coefficients are illustrated in Figure 19(a). A good agreement between simulated and measured results is obtained. The measured fractional impedance bandwidth for S11 < −10 dB is wider than 50% over a 7 to 12 GHz frequency range. Although we can observe that the measured reflection coefficient of the proposed antenna array deteriorates at 8.5 GHz and 10.5 GHz from Figure 19(a), it is still less than −10 dB. The main reason for the difference may be the influence of fabrication accuracy, especially the welding joint at the corner of the feeding network which is not standardized. The simulated and measured gain results are depicted in Figure 19(b) and show that the measured gain range is 14–19.75 dBi. The simulated and measured gain results share similar trends, but the measured gain is about 1.0 dB lower than the simulated gain. The main reason for this difference is fabrication error and material loss. Moreover, in the process of measurement, the differential circuit components, used for measuring the radiation characteristics of the purposed antenna, may also exhibit a negative effect. Therefore, we should pay attention to the effect of the external differential circuit components on the antenna gain during the measurement process.

The simulated and measured normalized radiation patterns in both the E-plane and H-plane at 8 GHz, 9.5 GHz,

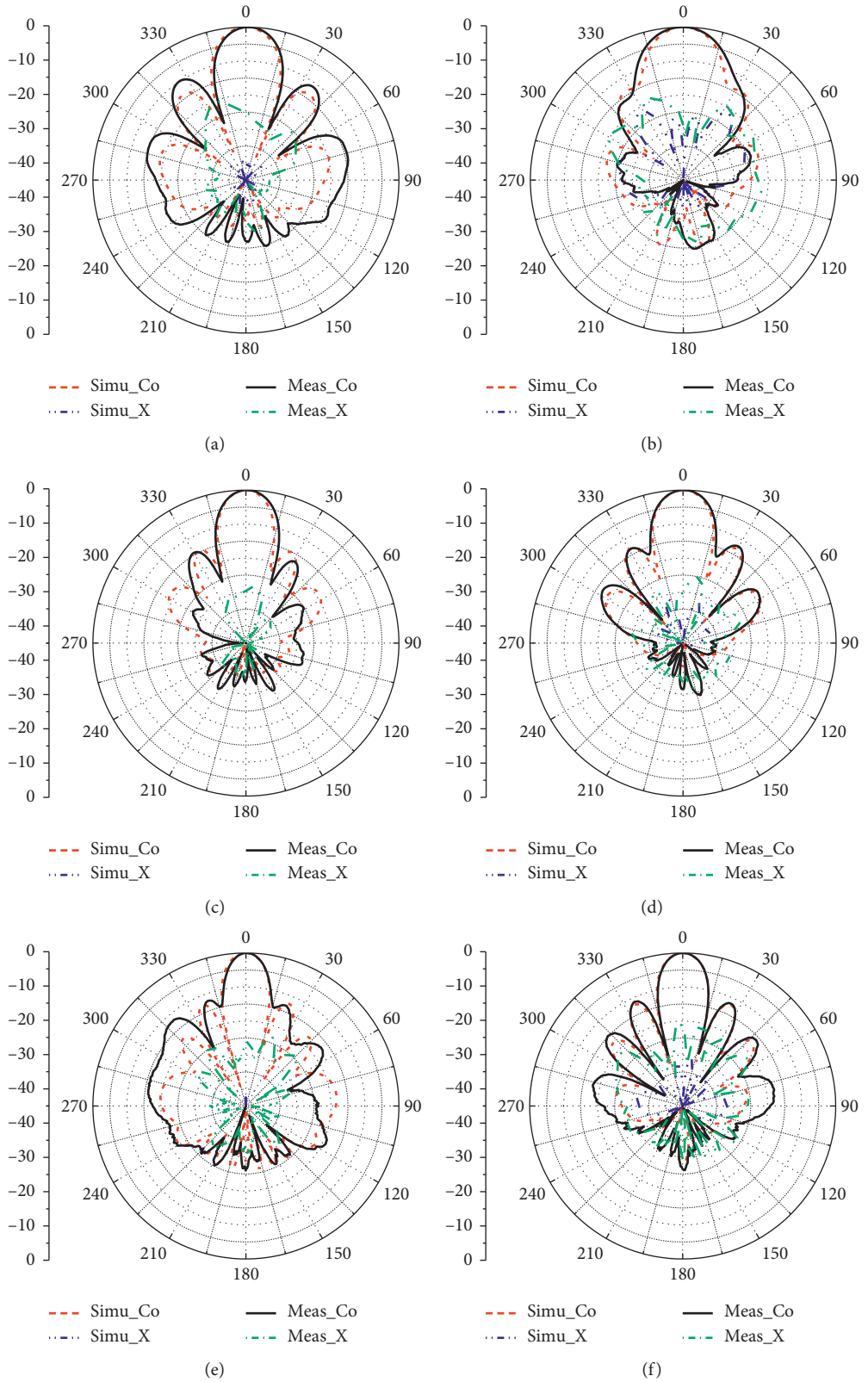


Figure 20: Simulated and measured co- and cross-polarization radiation patterns of the proposed antenna array at different frequencies. (a) E-plane at 8 GHz. (b) H-plane at 8 GHz. (c) E-plane at 9.5 GHz. (d) H-plane at 9.5 GHz. (e) E-plane at 11 GHz. (f) H-plane at 11 GHz.

Table 1: Comparison with other antenna elements/arrays.

| Ref. | Center freq. (GHz) | Elements | Size | Differential feeding | Impedance bandwidth (%) | 3 dB gain bandwidth (%) | Cross-pol. (dB) | Max. gain (dBi) | Max. radiation efficiency (%) |
|---|---|---|---|---|---|---|---|---|---|
| [5] | 2.42 | 1 | $1.13\lambda_0 \times 1.13\lambda_0 \times 0.01\lambda_0$ | Yes | 46 | N/A | −28 | 4.5 | N/A |
| [12] | 1.6 | 1 | $0.64\lambda_0 \times 0.64\lambda_0 \times 0.09\lambda_0$ | No | 17.2 | 17.2 | −20 | 8.8 | 90 |
| [13] | 2 | 1 × 4 | $3.75\lambda_0 \times 1.33\lambda_0 \times 0.25\lambda_0$ | No | 46 | 46 | −27 | 13.5 | 95 |
| [14] | 2.2 | 1 | $1.03\lambda_0 \times 1.03\lambda_0 \times 0.25\lambda_0$ | Yes | 50 | 50 | −20 | 7.9 | N/A |
| [15] | 10 | 1 | $0.8\lambda_0 \times 0.8\lambda_0 \times 0.6\lambda_0$ | No | 40 | 40 | — | 9.5 | N/A |
| | 9.45 | 4 × 4 | $3.18\lambda_0 \times 3.18\lambda_0 \times 0.57\lambda_0$ | No | 30 | 30 | — | 18 | N/A |
| [20] | 12 | 1 | $1.32\lambda_0 \times 0.92\lambda_0 \times 0.13\lambda_0$ | Yes | 51 | 51 | −30 | 9 | 93 |
| This | 10 | 1 | $1.67\lambda_0 \times 1.67\lambda_0 \times 0.33\lambda_0$ | Yes | 62 | 48 | −20 | 9.7 | 96 |
| work | 10 | 4 × 4 | $3.96\lambda_0 \times 3.96\lambda_0 \times 0.33\lambda_0$ | Yes | 50 | 38 | −20 | 19.7 | 96 |

and 11 GHz are shown in Figure 20. The measured results are consistent with the simulation results. Moreover, the antenna has a stable, unidirectional radiation pattern within the operational frequency band and shows a cross-polarization level less than −20 dB at boresight. However, because of the impact of the test environment and fabrication accuracy, there is a deviation between the measured and simulated results about the side lobes and the cross-polarization levels. In the demand of radar systems, the cross-polarization levels of the antenna have negligible effect on the performance of the radar systems. Thus, the proposed antenna fully meets the requirements of the indicator.

Table 1 shows the comparison between the proposed antenna and the previously reported antennas. Observations of Table 1 show that the proposed antenna has a wider impedance bandwidth compared to the reported antennas. Moreover, the proposed antenna has a higher gain compared to the reference antennas in [5, 12–14]. The gain of the cavity-backed slot antenna array in [15] is higher than the gain of the proposed antenna, but the cavity-backed slot antenna is heavy and costly and has a complicated fabrication process. Although the reflection surface of the proposed antenna element and the array takes a relatively large dimension, the size of the reflection surface has little effect on the performance of the antenna because of the introduction of the semiclosed cavity formed by the stereoscopic feeding structures. Therefore, compared to the antennas referred above, the proposed antenna has a wider impedance bandwidth, high gain, lightweight, and a more compact structure. Although the cross-polarization level of the proposed antenna is around −20 dB, which is average compared with that of other differential antennas, it has already met the application requirements of radar systems.

## 6. Conclusion

In this paper, a wideband differentially fed slot antenna element and a 4 × 4 antenna array are proposed and fabricated. Two rectangular slots are introduced to extend the impedance bandwidth by creating a new resonance point. A series of benefits are brought by using the stereoscopic feeding structure. Firstly, it can improve the beam offset and splitting of the radiation patterns by reducing the cross-polarization. Secondly, it can reduce the influence of the exciting structure and plays an important role in supporting the antenna structure. Thirdly, based on the stereoscopic feeding structures, a hierarchical feeding network is proposed to design a 4 × 4 differentially fed antenna array. This method maintains the wide impedance bandwidth and stabilizes the antenna's radiation pattern. The antenna element and 4 × 4 array prototype are fabricated and tested, which verifies the theory proposed in this paper and characteristics of wideband and high gain. All in all, the proposed antenna array is a valuable candidate for modern wideband radar systems.

## Data Availability

The data used to support the findings of this study are available from the corresponding author upon request.

## Conflicts of Interest

The authors declare that there are no conflicts of interest regarding the publication of this paper.

## Acknowledgments

This study was supported by the National University of Defense Technology.

## References

[1] K. L. Wong, *Compact and Broadband Microstrip Antennas*, Wiley, Hoboken, NJ, USA, 2002.

[2] D. Cavallo, W. H. Syed, and A. Neto, "Connected-slot array with artificial dielectrics: a 6 to 15 GHz dual-pol wide-scan prototype," *IEEE Transactions on Antennas and Propagation*, vol. 66, no. 6, pp. 3201–3206, 2018.

[3] S. Das and D. Mitra, "A compact wideband flexible implantable slot antenna design with enhanced gain," *IEEE Transactions on Antennas and Propagation*, vol. 66, no. 8, pp. 4309–4314, 2018.

[4] X. Zhang and L. Zhu, "Gain-enhanced patch antenna without enlarged size via loading of slot and shorting pins," *IEEE Transactions on Antennas and Propagation*, vol. 65, no. 11, pp. 5702–5709, 2017.

[5] C. Wang, Y. Chen, and S. Yang, "Bandwidth enhancement of a dual-polarized slot antenna using characteristic modes," *IEEE Antennas and Wireless Propagation Letters*, vol. 17, no. 6, pp. 988–992, 2018.

[6] J. J. Lee, S. Livingston, and R. Koenig, "Performance of a wideband (3–14 GHz) dual-pol array," in *Proceedings of the IEEE Antennas and Propagation Society Symposium*, vol. 1, pp. 551–554, Monterey, CA, USA, June 2004.

[7] Z. Yang, H. Jingjian, W. Weiwei, and Y. Naichang, "An antipodal Vivaldi antenna with band-notched characteristics for ultra-wideband applications," *AEU-International Journal of Electronics and Communications*, vol. 76, pp. 152–157, 2017.

[8] H. Malekpoor and S. Jam, "Improved radiation performance of low profile printed slot antenna using wideband planar AMC surface," *IEEE Transactions on Antennas and Propagation*, vol. 64, no. 11, pp. 4626–4638, 2016.

[9] Y. Shi, J. Liu, and Y. Long, "Wideband triple- and quad-resonance substrate integrated waveguide cavity-backed slot antennas with shorting vias," *IEEE Transactions on Antennas and Propagation*, vol. 65, no. 11, pp. 5768–5775, 2017.

[10] S.-H. Wi, Y.-S. Lee, and J.-G. Yook, "Wideband microstrip patch antenna with U-shaped parasitic elements," *IEEE Transactions on Antennas and Propagation*, vol. 55, no. 4, pp. 1196–1199, 2007.

[11] W. Hu, R.-N. Lian, Z.-Y. Tang, and Y.-Z. Yin, "Wideband, low-profile, dual-polarized slot antenna with an AMC surface for wireless communications," *International Journal of Antennas and Propagation*, vol. 2016, Article ID 7641382, 8 pages, 2016.

[12] S. X. Ta, K. E. Kedze, D. N. Chien, and I. Park, "Bandwidth-enhanced low-profile Antenna with parasitic patches," *International Journal of Antennas and Propagation*, vol. 2017, no. 5, Article ID 6529060, 11 pages, 2017.

[13] R. Lian, Z. Wang, Y. Yin, J. Wu, and X. Song, "Design of a low-profile dual-polarized stepped slot antenna array for base station," *IEEE Antennas and Wireless Propagation Letters*, vol. 15, pp. 362–365, 2016.

[14] Z. Tang, J. Liu, and Y. Yin, "Enhanced cross-polarization discrimination of wideband differentially fed dual-polarized antenna via a shorting loop," *IEEE Antennas and Wireless Propagation Letters*, vol. 17, no. 8, pp. 1454–1458, 2018.

[15] H. Yang, J. Lu, C. Lin, C. Song, and G. Gao, "Design of wideband cavity-backed slot antenna with multilayer dielectric cover," *IEEE Antennas and Wireless Propagation Letters*, vol. 15, pp. 861–864, 2016.

[16] H. Kang and S. Park, "Mushroom meta-material based substrate integrated waveguide cavity backed slot antenna with broadband and reduced back radiation," *IET Microwaves, Antennas and Propagation*, vol. 10, no. 14, pp. 1598–1603, 2016.

[17] Y. Cai, Y. Zhang, Z. Qian, and J. Liu, "A 16-element corporate-feed multilayer SIW cavity-backed slot antenna array," *IET Microwaves, Antennas and Propagation*, vol. 11, no. 12, pp. 1796–1802, 2017.

[18] X. F. Zhao, H. Z. Liu, L. Yi, S. G. Zhou, and C. Y. D. Sim, "A low VSWR and high efficiency waveguide feed antenna array," *Wireless Communications and Mobile Computing*, vol. 2018, Article ID 7867091, 7 pages, 2018.

[19] D. Wang, K. B. Ng, C. H. Chan, and H. Wong, "A novel wideband differentially-fed higher-order mode millimeter-wave patch antenna," *IEEE Transactions on Antennas and Propagation*, vol. 63, no. 2, pp. 466–473, 2015.

[20] C. Chen, C. Li, Z. Zhu, and W. Wu, "Wideband and low-cross-polarization planar annual ring slot antenna," *IEEE Antennas and Wireless Propagation Letters*, vol. 16, pp. 3009–3013, 2017.

[21] A. D. Johnson, J. Zhong, M. Livadaru, E. A. Alwan, and J. L. Volakis, "Tightly coupled dipole array with wideband differential feeding network," in *Proceedings of the 2018 IEEE International Symposium on Antennas and Propagation & USNC/URSI National Radio Science Meeting*, Boston, MA, USA, July 2018.